Nuclear Instruments and Methods in Physics Research A304 (1991) 1–11
North-Holland

Section I. Linac FEL experiments

First operation of a free electron laser using a ring resonator *

D.H. Dowell, M.L. Laucks, A.R. Lowrey, M. Bemes, A. Currie, P. Johnson, K. McCrary, L. Milliman, C. Lancaster, J. Adamski, D. Pistoresi and D.R. Shoffstall
Boeing Aerospace and Electronics, Seattle, Washington, USA

M. Bentz, R. Burns, J. Guha, R. Hudyma, K. Sun, W. Tomita and W. Mower
Rocketdyne Division of Rockwell International, Canoga Park, California, USA

S. Bender, J. Goldstein, A.H. Lumpkin, B. McVey and R. Tokar
Los Alamos National Laboratory, Los Alamos, New Mexico, USA

D. Shemwell
Spectra Technology Inc., Bellevue, Washington, USA

Invited paper

During the past year the Boeing free electron laser optical cavity was changed from a simple concentric cavity using two spherical mirrors to a much larger ring resonator. The new resonator is made up of two-mirror telescopes located at each end of the wiggler with a round-trip path length of approximately 133 m Each telescope consists of a grazing-incidence hyperboloid and a paraboloid. First lasing operation at 0.63 μm occurred on March 23 and 24, 1990. The lasing output was approximately seven orders of magnitude above the outcoupled spontaneous emission. The characteristics of the ring resonator are discussed. Lasing data is analyzed for the electron beam and ring resonator effects. Optical alignment techniques for the ring resonator are presented.

1. Introduction and description of FEL

The past year the Boeing free electron laser (FEL) optical cavity was changed from a simple concentric cavity using two spherical mirrors [1] to a much larger ring resonator [2]. The purpose of the new resonator is to test the operation and design of a grazing-incidence optical cavity for a high-power FEL.

The ring resonator was installed in the spring of 1988 and first aligned in the autumn of 1989. Preliminary electron beam tests in January and February, 1990, showed an irregular mechanical movement of the outcoupler. This was corrected, the ring refocused, and the optics cleaned from mid-February to mid-March. Resumed electron beam testing gave much improved operation and the ring successfully lased on March 23–24, 1990.

Table 1
Electron beam and Thunder wiggler parameters

Electron beam	
Electron beam energy	110 MeV
Repetition rate	2 Hz
Macropulse length	110 μs
Micropulse spacing	443 ns
Emittance (4 rms)	100–120π mm mrad
Macropulse energy jitter	0.5% to 0.75% FWHM
Micropulse energy spread	0.5% FWHM
Micropulse width	12 ps FWHM
Micropulse charge	3 nC
Thunder wiggler	
Length	5 m in 10, 50 cm sections
Wiggler period	2.18 cm
Number of periods	220 periods
Peak magnetic field	10.2 kG
Wiggler parameter	1.8 (peak)
Wiggler parameter	1 31 (rms)
Betatron period	5.6 m

* This research was done at: Boeing Physical Sciences Research Center, Mail Stop 2T-50, P.O. Box 3999, Seattle, WA 98124, USA.

0168-9002/91/$03.50

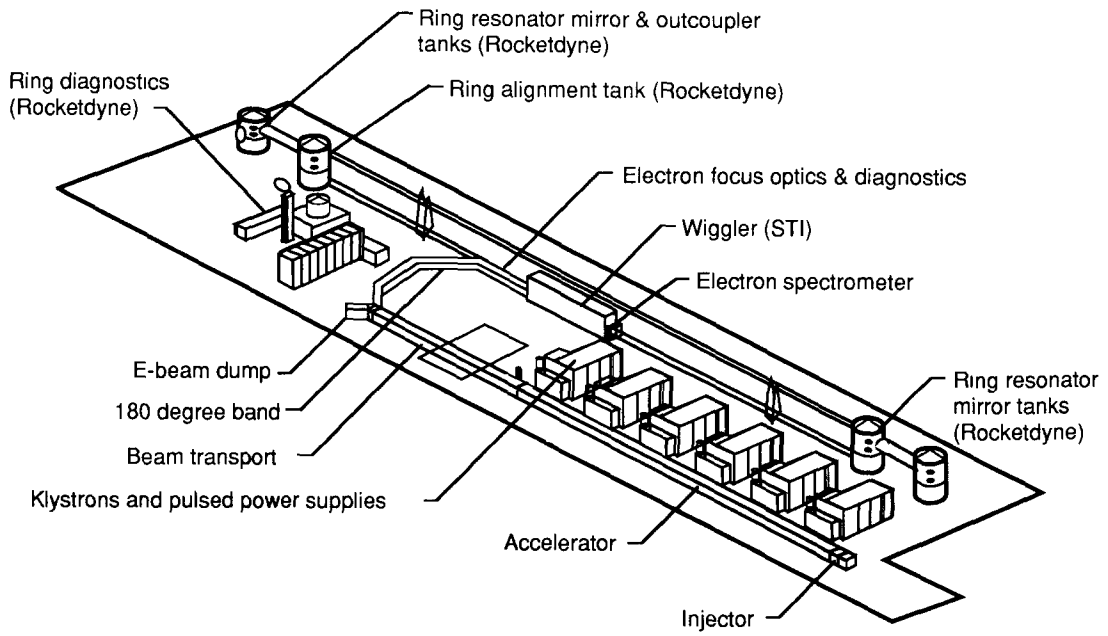

Fig. 1. Overview drawing of the Boeing free electron laser.

An overview drawing of the Boeing FEL is given in fig. 1. The electron accelerator has been discussed in detail elsewhere [3]. The more recent upgrades are discussed in another contribution to this conference [4]. Section 2 summarizes the electron beam parameters. The ring resonator is contained in the vacuum tanks located at each end of the wiggler and is described in section 3. A more detailed account of the ring resonator optical measurements is contained in ref. [5]. Section 4 presents the lasing test results and section 5 gives an analysis of the experiment. Future work and plans are discussed in the summary and conclusions section – section 6.

2. The electron accelerator

The electron accelerator has been described in detail elsewhere [3]. The recent work done to improve the beam quality is described in another contribution to this conference [4]. Space permits only listing the observed electron beam parameters in table 1.

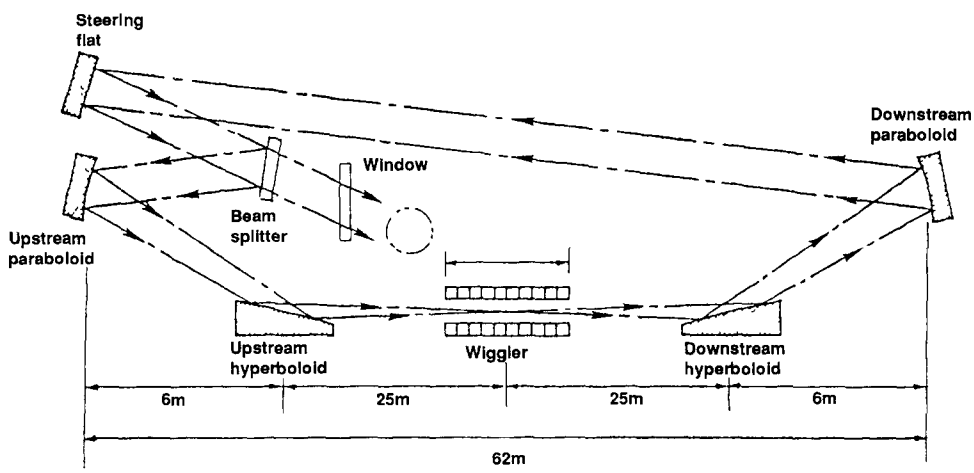

Fig 2. Grazing-incidence ring resonator.

Table 2
Ring resonator design parameters

Ring Rayleigh range	240 cm
Hyperboloid focal length	−105 cm
Paraboloid focal length	698 cm
Telescope magnification	7×
Hyperboloid–paraboloid spacing	600 cm
Roundtrip path length/time	133 m/443 ns

3. The ring resonator optical cavity

The optical resonator optics are contained in four large vacuum tanks, two at each end of the wiggler (fig. 1). The ring resonator parameters are given in table 2, and fig. 2 shows the ring resonator in more detail. The ring optics consists of a beam-expanding Galilean telescope at the downstream wiggler end, followed by an identical reducing Galilean telescope upstream of the wiggler. The beam-expanding hyperboloid mirror at grazing incidence has a negative focal length of 105 cm. This mirror is followed by a paraboloid with a 698 cm focal length. The beam in the resonator's return leg is collimated.

The ring resonator alignment is established using two helium–neon (HeNe) lasers. One is injected into the ring using a hologram, while the second uses a pellicle. The hologram beam is discussed here and the newly installed pellicle beam is explained in section 5. Fig. 3 illustrates the hologram beam injection system which produces both forward- and reverse-propagating beams. ("Forward" is in the same direction as the FEL optical beam.) Both beams are mode-matched to the resonator, and are produced by the same hologram by retro-reflecting the injection laser beam back through the same hologram. A second hologram is used to pick off a piece of the forward round-trip for analysis by a self-referencing interferometer (SRI) [5,6]. The reverse beam is turned out of the vacuum by a backward-facing mirror to measure the focal properties of the ring [5]. This is also shown in fig. 3.

Accurate determination of the ring resonator's foci locations, using the above technique, was done after the first lasing test of March through May. The results showed that instead of the round-trip focus for a forward-going beam occurring near or at the wiggler center, the focus was at the wiggler's entrance. In particular, the measurements made in June indicated that the horizontal round-trip focus was 267 cm and the vertical focus was 192 cm upstream of the 5 m wiggler's center. This meant the ring resonator was optically unstable during the March–May testing period. Since May, the downstream-telescope spacing has been decreased to move the ring focus closer to the wiggler center [5].

4. Free electron laser tests

This section outlines the process of matching and aligning the electron beam through the wiggler; the method for setting the cavity length to be synchronous with the electron beam; and the results of the lasing tests. The first lasing with the ring resonator occurred on March 23–24, and again on May 3–4.

4.1. Electron beam matching, alignment and diagnostics

Good electron beam quality at the wiggler is critical for optimal lasing at visible wavelengths. After the beam is brought around the 180° bend onto the wiggler axis, its emittance and stability are measured. If the emittance is too large, i.e. greater than 120π mm mrad, or has transverse positional jitter, then usually the beam has not been sized or steered properly into the bend, or the accelerator rf needs adjusting. Some of these effects are described more thoroughly in another contribution to this conference [4].

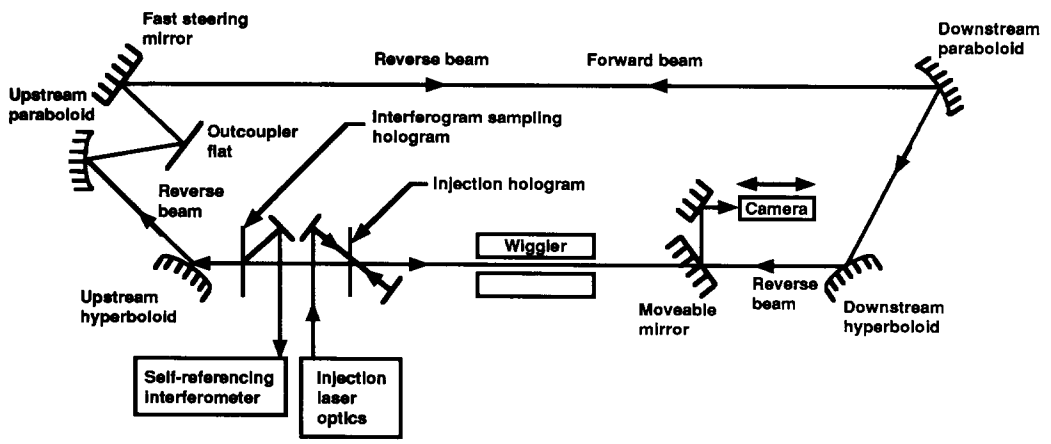

Fig. 3. Hologram alignment laser system.

The electron beam size and divergence are matched to the Thunder wiggler with the aid of a computer program which calls the electron beam optics code TRANSPORT, retrieves quadrupole settings from the data base, and uses the results of the two-screen emittance measurements. Once properly sized, the beam is allowed to drift into the wiggler and is viewed by the wiggler optical transition radiation (OTR) screens. Measurements of the beam size on the eleven wiggler screens placed every 50 cm (9 OTR and 2 alumina), confirm that the electron beam's diameter is constant along the wiggler [7].

The electron beam is aligned to the ring resonator optical axis using software marks indicating the centroids of the alignment laser on each of the wiggler screens. This is also done for the screens in front of the wiggler. Steering correctors in the Thunder wiggler are used to steer the electron beam onto these alignment marks. The positioning accuracy is approximately 50 μm.

After passing through the wiggler the electron beam is deflected downward by a magnetic spectrometer, transits a thin OTR screen and is stopped in a Faraday-cup beam dump (see fig. 1). The OTR light is brought out of the spectrograph's shielding using two fused-silica lenses and is relayed to a gated, intensified CID camera. The gate on this camera can be varied in both duration and delay to measure the energy of a single micropulse, or of groups of micropulses [4]. If the FEL extraction is above approximately 0.1%, then the lasing vs nonlasing centroid shift of the electron beam energy can be measured with this camera [8,9].

4.2. Cavity length setting

For lasing to occur the round-trip cavity length needs to match the electron micropulse spacing to within 50 to 100 μm. The technique involves the streak camera viewing the light from the outcoupler which is timed to pick out one of the micropulses of light. If the round-trip length does not equal the pulse spacing, the streak image will show smaller pulses offset in time due to ringdown light from the preceding pulses. This temporal spacing gives the amount the cavity is out of synchronicity with the electron beam. Unfortunately, since the electron beam pulse width is 12 ps (FWHM), the ringdown light from the preceding pulse begins to merge with the direct pulse at about 3 mm away from the proper cavity length. Therefore the pulse width limits the range for directly setting the cavity length, and an alternative, graphical method is used.

Fig. 4 illustrates the method used to determine the proper cavity length. The temporal spacing of the direct and ringdown pulses are plotted vs the outcoupler's z-position. This was done for positions out to 8 mm on either side of the expected zero-crossing. The data were

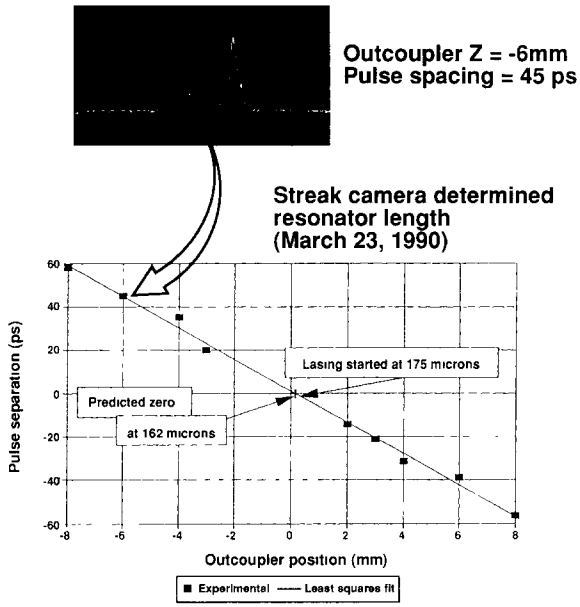

Fig 4. Ring resonator cavity length setting.

then fit with a straight line to produce the expected outcoupler position of 162 μm. The outcoupler was then moved to $z = 0$ μm and stepped in 10 μm intervals through the 162 μm position, while watching a photomultiplier tube (PMT) for some enhancement in the outcoupled light. When this was done on March 23, the ring began to lase at $z = 175$ μm. Since this occasion, the technique has correctly predicted the resonator length to ± 100 μm.

4.3 Lasing test results

The optical macropulse measured on March 23 is shown in fig. 5. This signal comes from a vacuum photodiode located on the control room optical table.

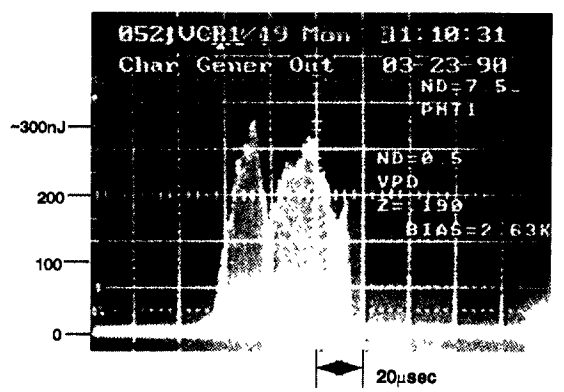

Fig. 5. Vacuum photodiode measurement of optical macropulse.

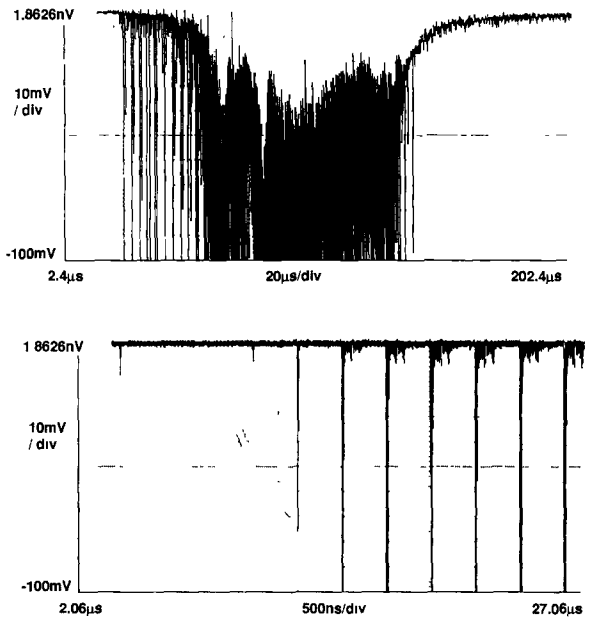

Fig. 6. Small signal gain (SSG) measurement.

The figure indicates that lasing occurred for 50 μs and exhibited at least a two-peak structure. The energy per micropulse peaked at approximately 300 nJ [5].

The next day, March 24, the ring resonator lased at similar power levels to those observed on March 23. Fig. 6 is a plot of a small signal gain (SSG) measurement using the PMT, again on the control room optics table. The lower scope trace is an expanded region of the upper PMT signal looking at the leading edge of the optical pulse. The leading two pulses suggest a very large SSG of over 1000% per pass; however, more measurements are needed to confirm this very preliminary result.

The SSG is very sensitive to the electron beam parameters listed in table 1. As shown by Goldstein [10], the SSG rapidly decreases when any of these parameters are degraded. This has been verified in subsequent runs.

On May 3–4 measurements were made to understand how the ring was lasing and to separate the electron beam effects from the ring resonator effects. Measurements were made of:

- the macropulse-integrated wavelength,
- optical output during the macropulse,
- streak spectrometer image of the time-resolved wavelength during the macropulse,
- stripline data of the electron beam energy, position and angular jitter during the macropulse.

Fig. 7 illustrates the wavelength of the FEL on May 3 for three separate macropulses collected over about 20 to 30 min. The wavelength is centered at 626 to 628 nm and is approximately 2 nm wide (FWHM).

Fig. 8 shows the optical output of the FEL on May 3 for four macropulses. The three scope pictures on the left are photodiode data collected for three macropulses. The histogram on the right was taken with the LANL streak spectrometer [9] operating in dual sweep streak mode. Multipeak structure is evident in both sets of measurements, and there is considerable variation from macropulse to macropulse. This variation comes from both the electron beam and limitations in the ring stabilization system.

The ring is stabilized by feedback control of the fast-steering mirror using the signal from a quadcell located at the wiggler center. An off-axis laser begins near the wiggler center and circulates around the ring, returning to the quadrant detector on the opposite side of the wiggler. Unfortunately, the present control circuit is limited to frequencies below approximately 30 Hz.

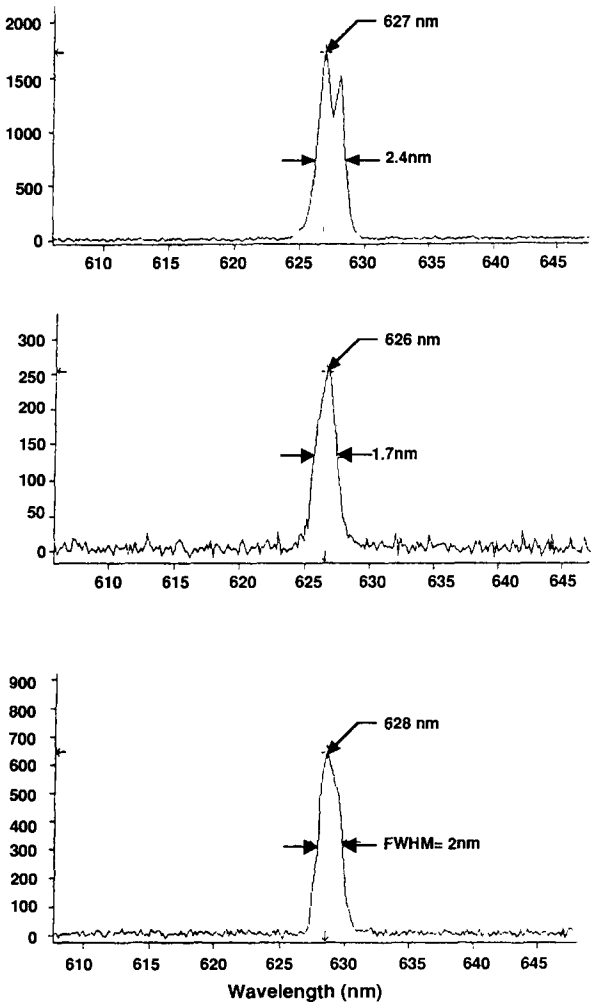

Fig. 7. OMA spectra for three macropulses.

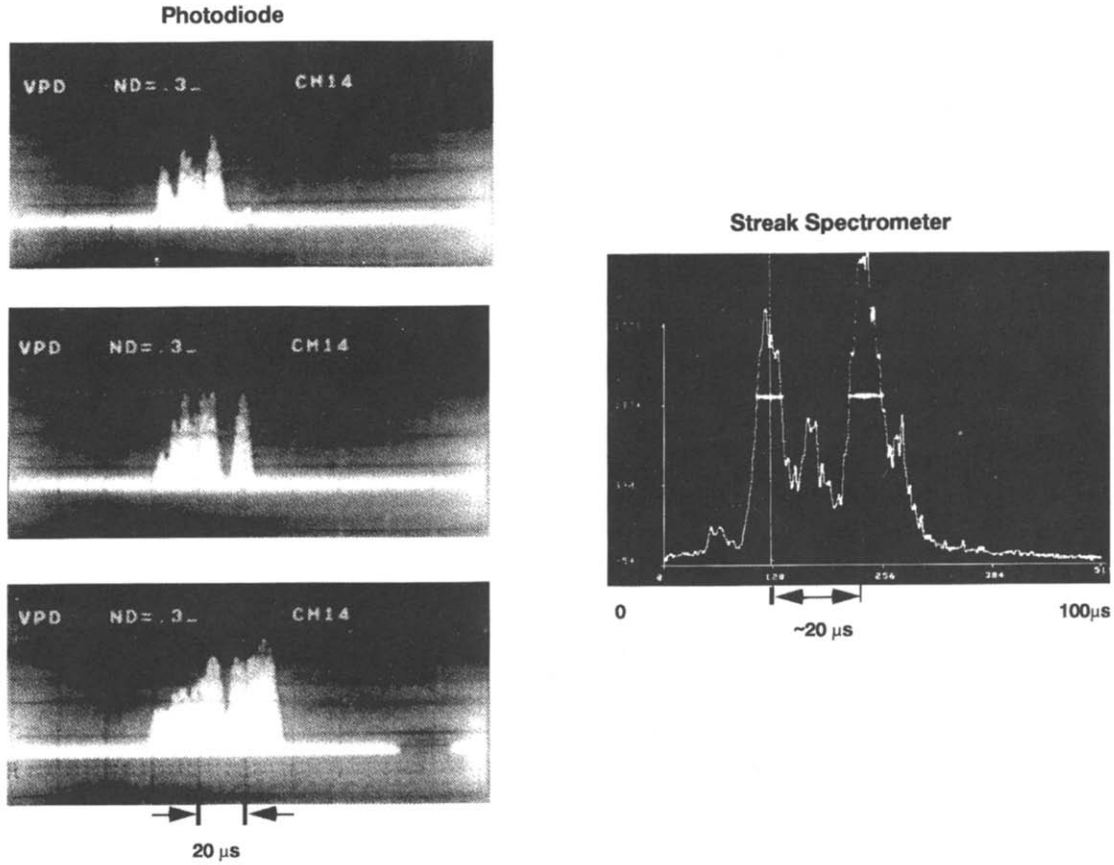

Fig. 8. FEL output measurements on May 4.

The residual peak-to-peak amplitude of the optical beam motion is between 300 and 500 μm, and has two components, one near 50 Hz and the other near 100 Hz. Work is in progress both to increase the control loop bandwidth and to eliminate vibration sources.

Fig. 9 gives the streak spectrometer image data for the FEL optical output. The horizontal axis is wavelength, with increasing wavelengths to the left. The vertical axis is time, increasing into the macropulse downward. There are some differences, but these mea-

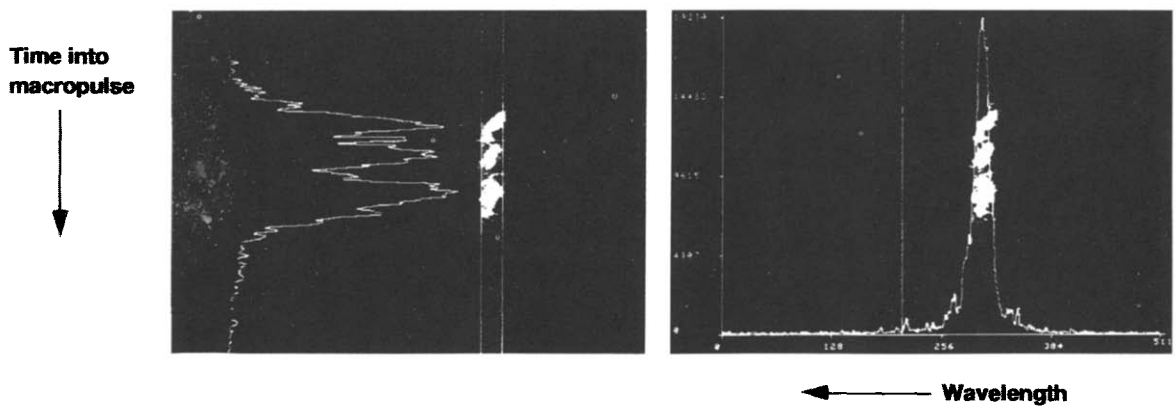

Fig. 9. Streak spectrometer image of FEL output.

surements exhibit a similar time-dependent structure to the vacuum photodiode output of fig. 5, and the photodiode and streak spectrometer data in fig. 8. Major structures in the FEL output are present with both 10 and 20 μs periods.

Stripline data were also taken on May 3 and 4 to determine if these structures were due to electron beam variations during the macropulse. Such effects were often present in the early concentric cavity data [9]. Stripline measurements are shown in fig. 10 for three striplines, 21, 22 and 23 [4]. Striplines 22 and 23, located in front of the wiggler, are separated by a 250 cm drift and between them can measure both offsets in the electron beam position and angle changes in front of the wiggler. These striplines are essentially featureless and cannot identify the source of the FEL's structure. The micropulse centroid energy, as determined by stripline 21, does change during the macropulse in essentially three regions. In the first 25 μs, the beam energy is roughly 0.25% high, then the mean energy drops to its proper value but oscillates with a 10 μs period, and finally the energy is flat for the remaining 40 to 50 μs.

This energy variation is compared with a series of photodiode measurements in fig. 11. The energy stripline data are plotted above the diode output with the same horizontal time scale. Except possibly for some modest correlation with the electron beam energy jitter in the first 20 μs of lasing, there are no definite similarities between the energy variations and the lasing structures. It is also peculiar that the lasing stops prematurely before the macropulse ends. The May 3–4 measurements then suggest much of the lasing effects are caused by the ring resonator.

5. Analysis and discussion of FEL data

A persistent feature of lasing is the highly structured output. This structure could be attributed either to the variations in the electron beam, or to a resonator walking mode. This stripline data does not indicate a strong correlation with the electron beam energy. Certainly there is no indication of the 10 to 20 μs structure in the position or angle of the electron beam going into the wiggler. Therefore it is necessary to investigate the ring resonator dynamics.

Ring resonator walking behavior is compared with the concentric cavity in fig. 12. The calculations give the pass-to-pass centroid motion at the wiggler. The vertical

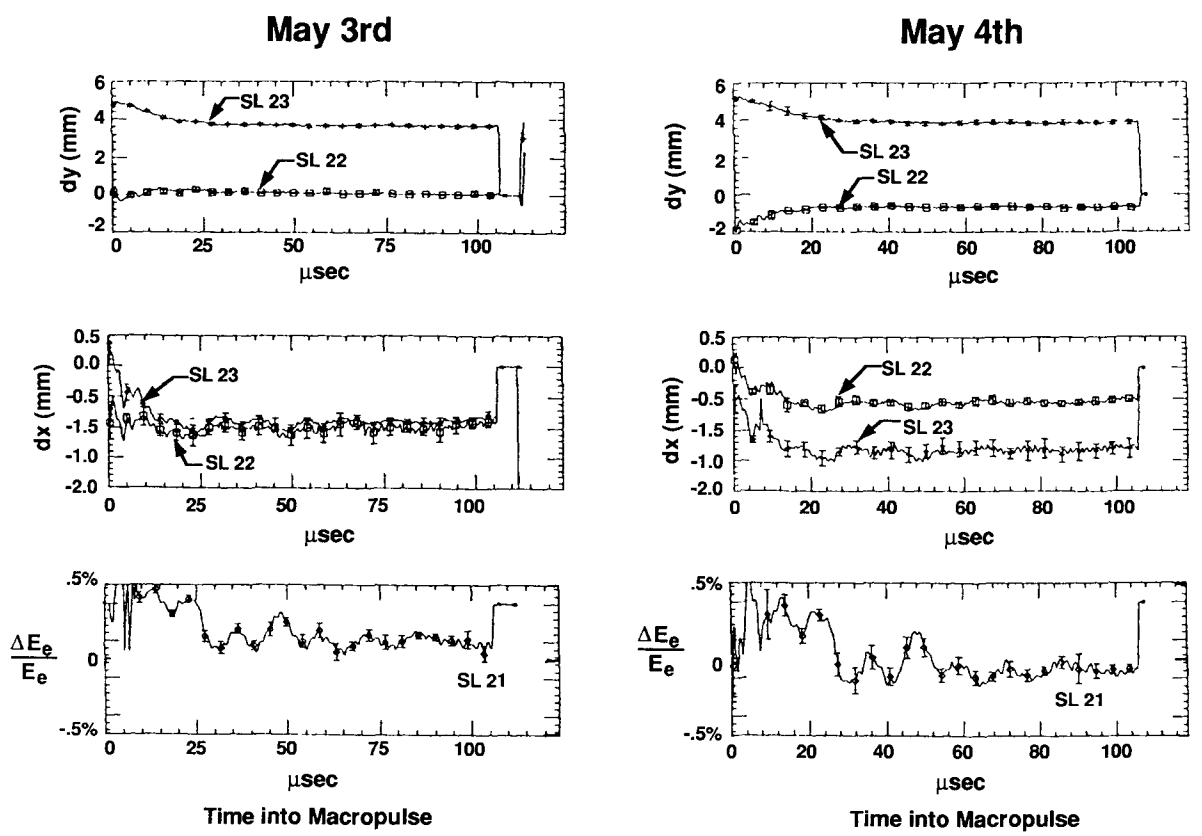

Fig. 10. Electron beam stripline data on May 3–4.

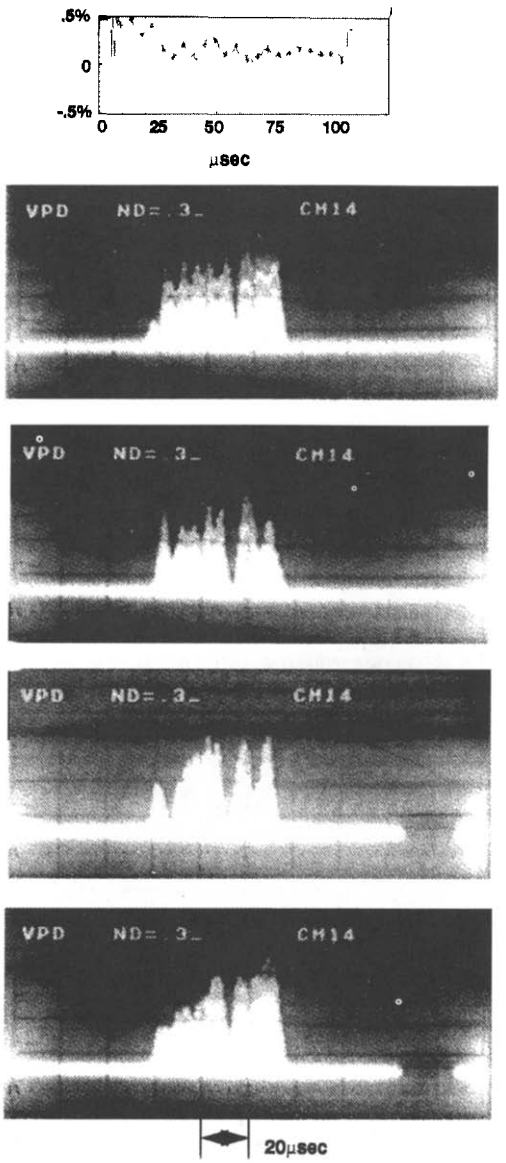

Fig. 11. Comparison of FEL output with electron beam energy jitter

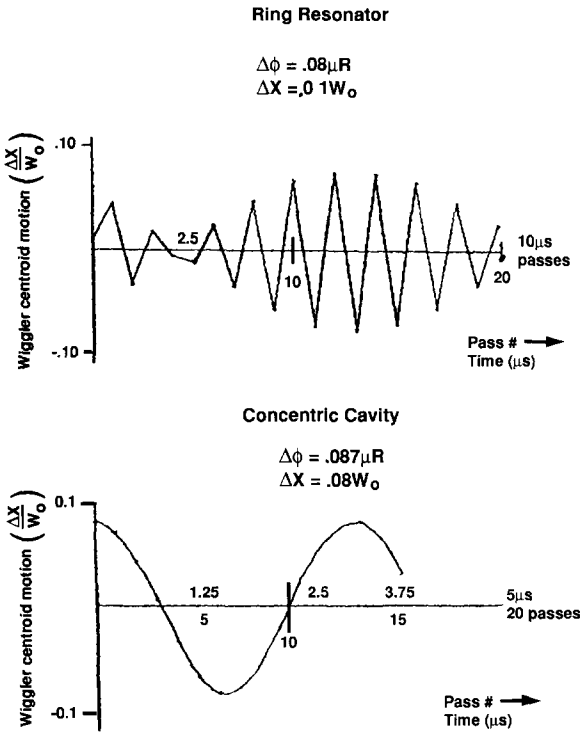

Fig. 12. Concentric cavity vs ring resonator walking behavior.

scales are in units of the beam waist size. The amplitude of the concentric cavity walk is similar to that of the ring resonator. The main difference is that the concentric cavity oscillates slowly about the optical axis, whereas the ring jumps from side to side.

Fig. 13 shows the resonator walking-mode calculation and the energy jitter with the streak spectrometer data. This figure directly compares two possible sources for the structural FEL output. The calculation above the data is similar to that shown in fig. 12, but has been

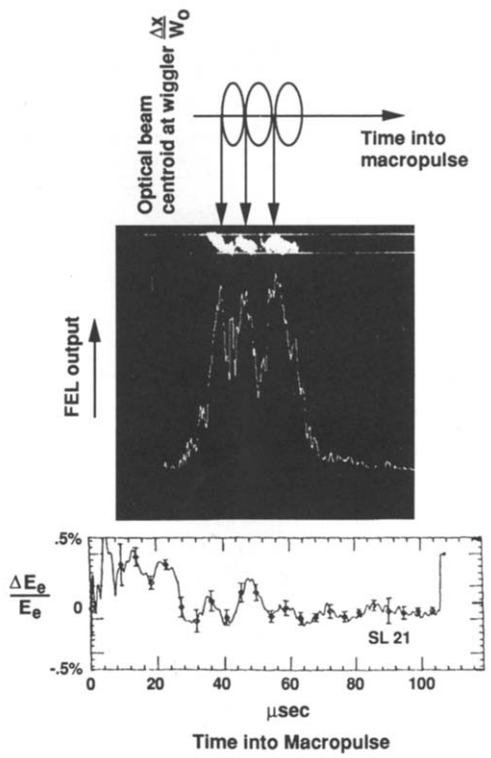

Fig. 13 Comparison of FEL output with walking calculation and electron beam energy variation

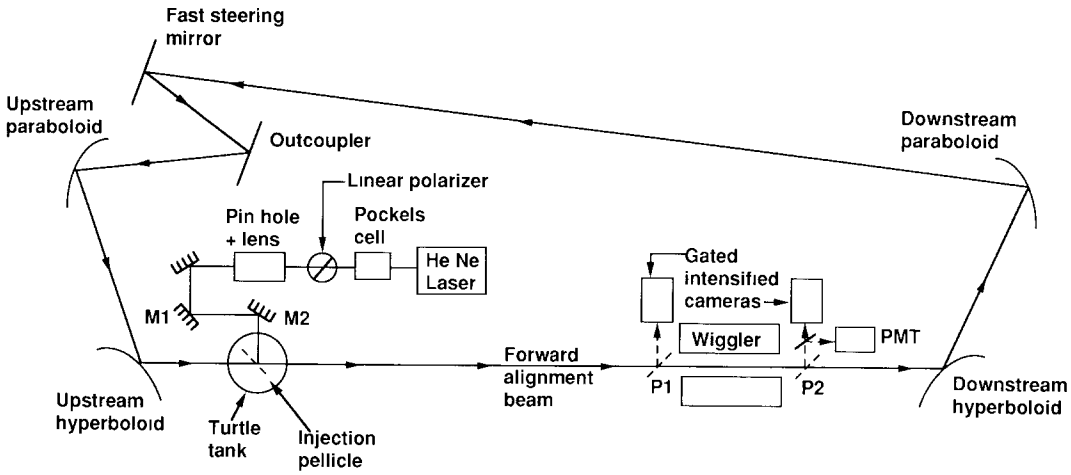

Fig. 14. Layout of the chopped–pellicle beam system.

shifted so the zero-amplitude points line up with the peaks in the FEL output. The 17-pass period of the walking is shown by the envelope. This figure suggests the structure could easily be due to the ring's walking mode. Lasing begins where the photon beam dwells for a few passes on the wiggler axis, but then, as the mode evolves, walks in larger and larger excursions on either side of the electron beam. As the walk amplitude grows, overlap with the electron beam is lost and the FEL output drops. Later in the macropulse the mode walks back to the wiggler axis and lasing again builds only to decline again approximately 10 μs later when the mode envelope is large again. Since the ring walking jumps from one side to the other, the light from pass to pass quickly diverges from the electron beam axis. For the particular case shown in fig. 13, the FEL passes through three mode periods before the end of the macropulse.

However, an alternative explanation is given below the streak data. Here the electron beam energy during the macropulse is plotted and suggests that the three structures are correlated with the energy fluctuations of the electron beam. But it remains very curious that the lasing stops when the electron beam energy is the flattest. A possible explanation would involve the nonisochronicity of the 180° bend. The nominal value is approximately 4.4 ps per percent of energy change. For the observed peak-to-peak energy slew of 0.25%, the micropulse spacing could change by about 1 ps. This is enough for the ring to stop lasing.

These effects clearly demonstrated the need for better experimental understanding of the ring's pass-to-pass alignment. Therefore, in addition to the hologram alignment laser discussed above, a new alignment scheme was implemented. The layout for this laser system is drawn in fig. 14. A second laser is injected into the ring using a thin pellicle and is focused at the wiggler center. It can be aligned to the wiggler axis using the mirrors, M1 and M2. The beam is chopped at 2 Hz into 200 ns long pulses by a pockels cell located between the HeNe laser and the spatial filter/lens combination. Two other pellicles, P1 and P2, located at each end of the wiggler can be inserted into the beamline to reflect a small portion of the injected laser light. The light from these sampling pellicles is directed into two gated, intensified CID cameras. Roughly 5% of the light from the downstream pellicle, P2, is also reflected into a photomultiplier tube (PMT) to measure the ringdown losses.

A typical ringdown pulse train from the PMT is shown in fig. 15. The 200 ns injected beam is the first pulse, followed by a series of successive pass pulses

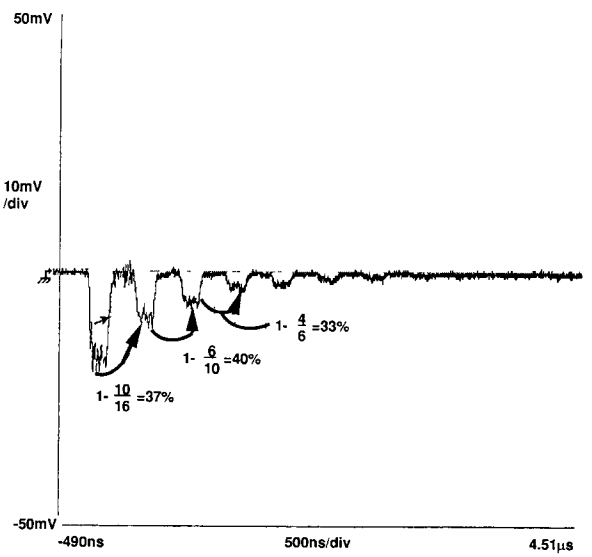

Fig. 15. Ringdown measurement using chopped–pellicle beam and PMT at sampling pellicle, P2.

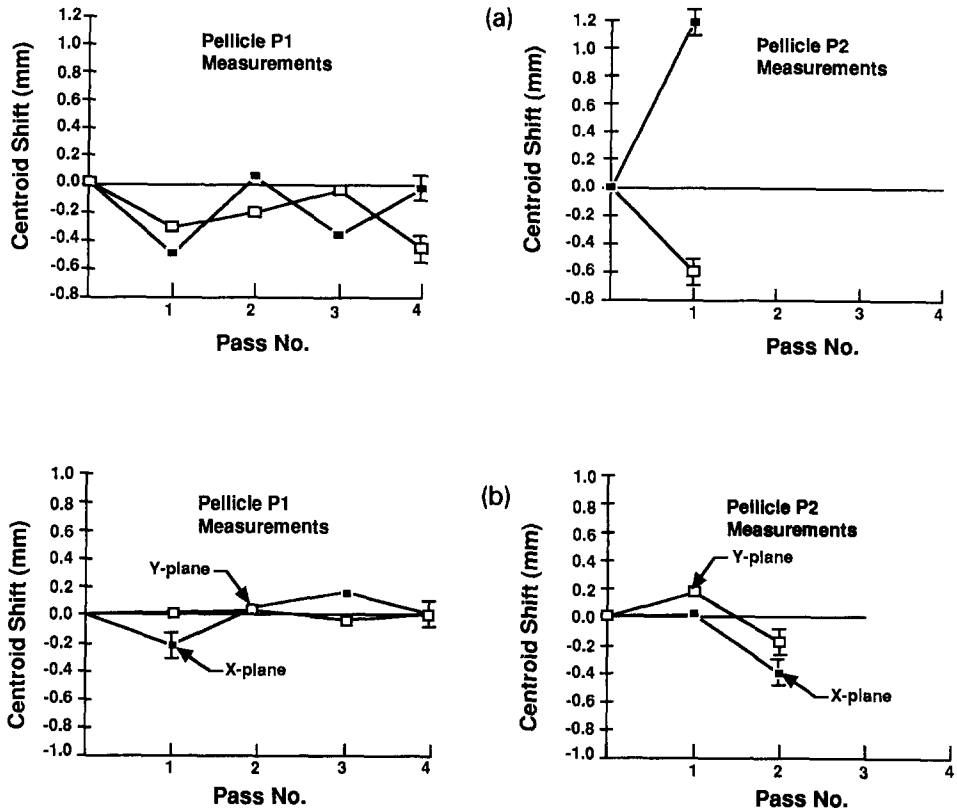

Fig. 16. Gated, intensified camera measurements of the pass-to-pass alignment before (a) and after (b) tip/tilts of downstream paraboloid and outcoupler

spaced at the 443 ns round-trip time of the ring. The round-trip ring losses are between 35% and 40%.

The transverse positions of these various round-trip beams at the pellicle locations, P1 and P2, are determined by the gated cameras. Adjusting the gate delay in 443 ns intervals (the ring round-trip time) allows the cameras to view up to the fourth round-trip beam before the light becomes too faint. Fig. 16 plots the centroid locations of the optical beam vs pass number around the ring. The positions are relative to the location of the injected beam. The pass-to-pass oscillatory motion duplicates the side-to-side oscillations calculated in fig. 12.

Using this new diagnostic tool, the pass-to-pass oscillations are minimized by steering the optical beam on the ring resonator backleg. In particular the downstream paraboloid is tipped and tilted along with the outcoupler to make the multipass centroids align to the wiggler center line. This should help eliminate one possible cause of structure in the FEL's output.

6. Summary and conclusions

The initial results of operating a FEL with a grazing-incidence ring resonator exhibit a structured optical output. Preliminary measurements indicated a small signal gain of several hundred percent; however, the energy output was quite low. Experiments performed during lasing indicated that this structure, as well as limited extraction, was not simply an electron beam effect; therefore work has been concentrated on the resonator's pass-to-pass alignment. The explanation that approximately 17 to 20 pass transverse walking mode structures and limits the output is supported by the data. An additional alignment laser with a chopped beam clearly demonstrated the presence of the side-to-side walk, and provides a means for correcting it by tipping the downstream paraboloid and outcoupler.

Experiments are in progress to demonstrate that this improved alignment results in more uniform output and higher extractions. Near-term plans include independently aligning the upstream and downstream telescopes. Presently the upstream telescope is compensating for misalignments in the downstream one.

Acknowledgements

This work is support by US Army Strategic Defense Command under contract DASG60-87-C-0011.

References

[1] K.E. Robinson, D.C. Quimby and J.M. Slater, IEEE J. Quantum Electron. QE-23 (1987) 1497.

[2] S.V Gunn and K.C. Sun, Proc AIAA 19th Fluid Dynamics, Plasma Dynamics Laser Conf., 1987, AIAA-87-1280

[3] A. Yeremian et al., Proc. 1989 IEEE Particle Accelerator Conf., pp. 657–659.

[4] D.H. Dowell et al., these Proceedings (12th Int. FEL Conf., Paris, France, 1990) Nucl. Instr. and Meth. A304 (1991) 336.

[5] M.L. Laucks et al., ibid., p. 25.

[6] R. Hudyma and L. Eigler, Computer-aided alignment of a grazing incidence ring resonator for a visible wavelength free electron laser, Int. Lens Design Conf., SPIE 1354 (June 1990) to be published.

[7] D.H. Dowell, J. Adamski, A.R. Lowrey and A.H. Lumpkin, Proc. 11th Int. FEL Conf., Naples, FL, USA, 1989, Nucl. Instr. and Meth. A296 (1990) 351.

[8] B. Tokar, L.M. Young, A.H. Lumpkin, B.D. McVey, L.E. Thode, S.C. Bender, K.C.D. Chan, A.D. Yeremian, D.H. Dowell, A.R. Lowrey and D.C. Quimby, ibid., p. 115.

[9] A.H. Lumpkin, R.L. Tokar, D.H. Dowell, A.R. Lowrey, A.D. Yeremian and R. Justice, ibid., p. 169;
A.H. Lumpkin, ibid., p. 134.

[10] J.C. Goldstein, R.L Tokar, B.D. McVey, C.J. Elliott, D.H. Dowell, M.L. Laucks and A.R. Lowrey, these Proceedings (12th Int. FEL Conf., Paris, France, 1990) Nucl. Instr. and Meth. A304 (1991) 622.

[11] R.L. Tokar, B.D. McVey, L.E. Thode and G.M. Gallatin, IEEE J. Quantum Electron. QE-25 (1989) 73.